Proceedings of the ASME 2010 3rd Joint US-European Fluids Engineering Summer Meeting and 8th International Conference on Nanochannels, Microchannels, and Minichannels
FEDSM-ICNMM2010
August 1-5, 2010, Montreal, Canada

FEDSM-ICNMM2010-30225

EXPERIMENTAL CHARACTERIZATION OF AIR-ENTRAINMENT IN A PLUNGING WATER JET SYSTEM USING PARTICLE IMAGE VELOCIMETRY (PIV)

Xiaoliang Qu
Department of Mechanical Engineering
China University of Petroleum, Beijing
P. R. China
xqu@pi.ac.ae

Afshin Goharzadeh
Department of Mechanical Engineering
The Petroleum Institute, Abu Dhabi
United Arab Emirates
agoharzadeh@pi.ac.ae

Lyes Khezzar
Department of Mechanical Engineering
The Petroleum Institute, Abu Dhabi
United Arab Emirates
lkhezzar@pi.ac.ae

Arman Molki
Department of Mechanical Engineering
The Petroleum Institute, Abu Dhabi
United Arab Emirates
amolki@pi.ac.ae

ABSTRACT

This paper presents a detailed experimental study of a plunging jet on a free liquid surface. An experimental characterization facility is designed and constructed for generating a vertical round water jet impinging on a free surface of a pool. The experimental analysis focuses on the jet penetration depth, its relation to impact velocity V_j and free jet length L_j. Present results are compared with previous studies. The flowmap for four different regimes, in terms of impact jet velocity is obtained. The details of the two-dimensional velocity field below the pool liquid free surface under a no-entrainment regime, is obtained using Particle Image Velocimetry (PIV) and reveals the entrainment behavior of the impinging jet flow below the interface.

INTRODUCTION

A variety of industrial processes such as aeration of chemical reactions, pouring process of liquids in containers and agitation of molten liquid phase involve complex two phase flow generated from an impinging jet on a liquid surface [1].

Understanding the mechanism of jet injection on free liquid surface has direct impact on equipment design in the energy industry such as emergency cooling injections in nuclear reactors or oil spill contaminant and recovery. To date, the majority of studies published on plunging jet flow on a free water surface have been focused on the average and global dynamic behavior of air/water mixture under a free surface of water. Such studies have considered the dynamic of air entrainment below the free surface and four major regimes related to the concentration of bubbles in water were identified: no-entrainment, incipient entrainment, intermittent entrainment and continuous entrainment.

Averaged time parameters, such as liquid jet depth penetration, bubbles size distribution, and void fraction, have been addressed and reported previously notably by Schmidtke *et al.* [2], Bonetto & Lahey [3] and Chirichella *et al.* [4]. The gas entrainment and generation of gas bubbles below the liquid pool surface is controlled by several parameters such as the liquid viscosity, the jet surface topology prior to impact and its velocity at impact and the liquid motion induced below the liquid pool free surface. However, detailed knowledge of the velocity field distribution below the liquid pool surface which could contribute to the understanding of the entrainment of gas bubble generation process is lacking and has not been explicitly measured. In addition, such information would be very useful for testing computational multiphase flow models [5-8].

The objective of the present work is to conduct a systematic experimental study of a plunging round water jet on a liquid pool. The experimental setup with the flow visualization system used and the corresponding image processing techniques are described in the next section. The result section discusses the regime map of four different flows (no-entrainment, incipient, intermittent and continuous entrainment), the characteristics of jet penetration depth for several exit jet velocities and the velocity field distribution under the free surface of the jet using PIV.

EXPERIMENTAL SETUP

The experimental setup is shown in Figure 1. The experiments were performed in a 0.3m x 0.3m x 0.5m

rectangular tank fabricated from transparent acrylic sheets for the purpose of flow visualization. A re-circulating flow was generated using a centrifugal pump, where water, used as the working fluid, was pumped out of the tank and then re-injected into the tank by a vertical thin-walled round nozzle made from aluminum with an inner diameter of d_0=6mm and length of L=0.5m. The vertical nozzle was supported by a frame fabricated from aluminum profiles and carefully aligned by means of a plume line. Throughout the experiments, the water level was kept constant at a height of H=0.42m.

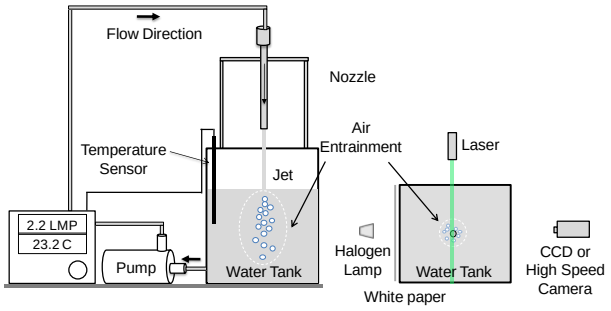

(a) schematic of experimental setup.

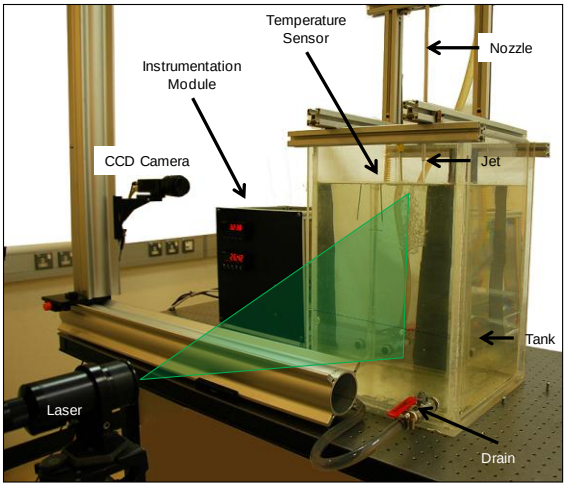

(b) flow visualization system.

Figure 1: Experimental setup.

The flow rate was controlled using a needle valve positioned downstream of the pump and measured by a paddle wheel flow meter (Omega model FTB603). The flow meter uses an infrared electro-optical transmitter and receiver to output a square wave signal with a frequency proportional to flow rate with an accuracy of ±3%. The fluid temperature for each experimental case was monitored by a K-type naked-bead thermocouple. The readings of flow rate and temperature were displayed on two electronic readout indicators. Efforts were made to conduct the experiments at a constant average temperature of 26°C.

FLOW VISUALIZATION

The experimental procedure involved flow visualization using digital imaging and Particle Image Velocimetry (PIV) in order to characterize different flow regimes, obtain the bubbly flow penetration depth for continuous entrainment flow regime and measure 2D velocity distribution below the free surface for no-entrainment regime.

Digital Imaging

Experiments were carried out for different nozzle heights L_j and volumetric flow rates Q_j. The water velocity V_0 at the nozzle exit ranged from 0.4m/s to 3.0m/s.

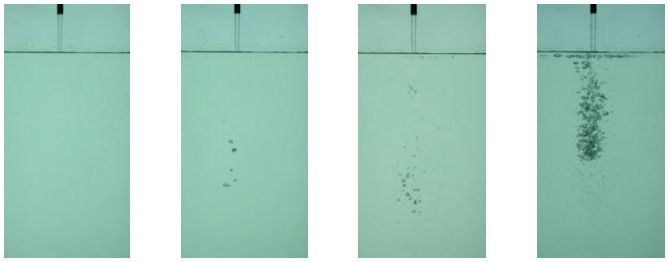

Figure 2: Digital photography of flow regimes: (a) no-entrainment, (b) incipient entrainment, (c) intermittent entrainment, (d) continuous entrainment.

Four different air entrainment regimes below the water pool free surface, identified by Chirichilla et al. [4] and discussed by Schmidtke et al. [2] were observed in the experiments. As shown in Figure 2, each entrainment regime was observed and captured using a digital SLR camera with an 18-200mm lens mounted on a sturdy tripod to minimize camera vibration. It was observed that the images taken at a shutter speed of 1/400s produced sharp results of the required quality.

To extract the bubbly flow penetration depth for the continuous entrainment regime, a high-speed camera (Photron model SA3) was used to capture instantaneous images. A sequence of images of the region below the water surface was taken. Images were recorded using a 50mm lens at a rate of 500Hz over a time period of 5.462s, resulting in a series of 2,727 images. Throughout the experiments a custom made array of high-power fluorescent lights was used to provide suitable and uniform backlighting.

Image Analysis

To measure the flow penetration depth, 2,727 frames of images were captured using a high-speed camera for each case of nozzle height and flow rate. A steel ruler with a precision of 0.5mm was used as the reference scale in each recorded image. It was visually observed from the recorded frames, that the depths which the bubbly plume reached, showed very small changes between each sequential frames; hence an averaged image containing 2,727 frames was generated in order to obtain

an accurate estimation of the average penetration depth for each case over a period of 5.454s (Figure 3).

Image processing was carried out by utilizing the Image Processing Toolbox in MATLAB. The multi-step process first involved reading and averaging 2,727 frames of images (Figure 4(a)). The next steps involved conversion of the averaged image to grayscale mode (Figure 4(b)), subtraction of its background (Figure 4(c)), and conversion into a binary image (Figure 4(d)). Conversion to binary image resulted in a clear contour of the bubbly jet, thus aiding the depth penetration calculation. An arbitrary threshold value of 0.15 was used for converting grayscale images to binary. As a final additional step, penetration depth was measured using the ruler tool in Photoshop.

To validate the selection of the arbitrary threshold value, the results were compared to the penetration depth defined by another approach: for each time step the lowest large bubble (d > 1mm) was identified and its depth was recorded as an instantaneous penetration depth. It was found that the values from the two approaches were quite almost identical with an error less than 5%.

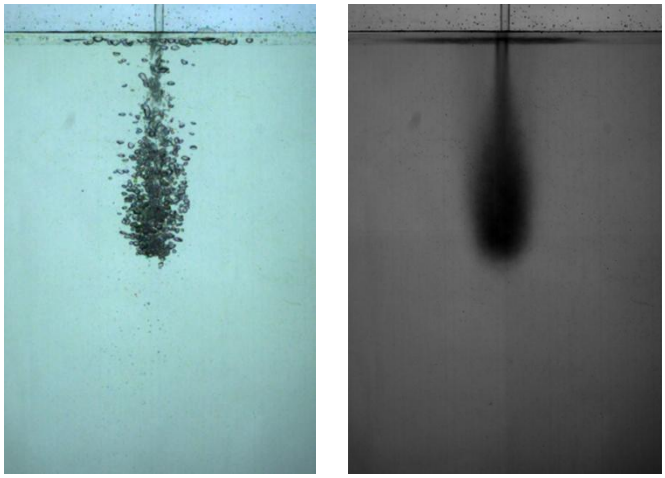

(a) Single recorded image. **(b)** Averaged image of 2,727 frames.

Figure 3: Photographs of continuous entrainment regime.

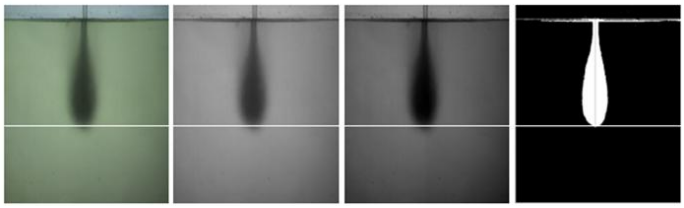

(a) Original **(b)** Grayscale **(c)** Background subtracted **(d)** Binary image

Figure 4: Image processing steps of averaged images.

Velocity Field Using PIV

Using PIV, all planar flow field measurements were taken in the central vertical plane of the rectangular tank. To illuminate this measurement plane, a vertical laser sheet was projected, with a charge coupled device CCD camera installed perpendicular to this plane to record the particles' motion, as illustrated in Figure 1. The water was seeded with polyamide particles tracers with a diameter of 22 μm and density of 1.016 g/cm^3 for flow visualization. The PIV flow field measurements were undertaken, for the non-entrainment regime, within two different regions: (i) the entire region of the tank, from the interface to the bottom of the tank, (ii) zoomed region below the water-air interface.

The flow was observed with a field of view of 30x50 mm^2. The tracers' density was 15–20 particles per interrogation area. A Yag-laser was used as the light source for planar PIV measurements having a maximum power output of 500 Watts at a wavelength of 532 nm. A cylindrical lens was used to generate a light sheet of approximately 1 mm thickness. The time between each couple of images was 1,000 ms. The pulse separation time was adjusted to 125 ms. Full-frame images of 1,600x1,186 pixels were acquired and transferred to a computer via a frame grabber.

Using the Flow Manager software developed by Dantec Dynamics, the 2D PIV image was divided into 64 x 64 pixels size sub-regions using a multi-grid correlation process with 50% overlap. The average particle velocities were calculated using 50 images coupled with the cross correlation method. The spurious vectors calculated and based on the local median filtering were less than 3%. No smoothing data were used for the velocity calculation.

PIV measurement accuracy can be influenced by a range of error sources that include, for example, tracer density, particle displacement, velocity gradients in the interrogation windows, background noise of the recordings, and quantization level of the camera. In Raffle et al. [9], a detailed discussion of the influence of such error sources is given. Additionally, near wall measurements using PIV are often difficult and characterized by large errors and uncertainties due to potential difficulties encountered with light scattering from wall boundaries and lack of seed particles in the near wall region.

RESULTS

The results of the experiments consist of the flow map regime, the jet penetration depth followed by a description of the planar velocity measurements below the pool free surface. The present results are discussed and compared against previously published work [2].

Flowmap Regime

The Reynolds number of the jet at nozzle exit was calculated based on the nozzle diameter thus:

$$R_e = \frac{\rho_l d_0 V_0}{\mu_0} \quad (1)$$

Where ρ_l is the liquid density, d_0 is the nozzle inner diameter and V_0 is the liquid jet velocity at the nozzle exit and μ_0 the viscosity of the liquid.

For the given range of nozzle exit velocities, Reynolds numbers were calculated to be between 2,400~18,000. If the critical Reynolds number for pipe flow is taken equal to 2,300 and considering the length of the nozzle pipe, a fully developed turbulent pipe flow would be expected at the nozzle exit.

Figure 4 shows the flowmap regimes. Each data point characterizes an experimental measurement for a given jet length and a nozzle velocity, resulting in a calculated impact velocity obtained by the following equation [1]:

$$V_j = \sqrt{V_0^2 + 2gh} \quad (2)$$

It was observed that the temperature difference between any two data points in the map was within 1°C, thus minimizing the temperature influence on the entrainment and flow motion. The jet falling length was varied between 0.01 m and 0.2 m. According to Equation 2 this yielded impact velocities V_j between 0.66 m/s and 3.59 m/s.

The obtained flowmap regime is in good agreement with the pervious flowmap established by Schmidtke et al. [2]. The boundary between different regimes is demarcated using trend lines for which the impact velocity V_0 remains constant. It can be seen that continuous entrainment becomes the dominant mode as L_j increases. The flow visualization observations also revealed that intermittent entrainment is associated with free intermittent liquid jet break up prior to impact and that the break up is responsible for intermittency.

Penetration depth

The penetration depth is defined as the lowest point of the plume where the velocity of the bubble becomes zero and buoyancy force is dominant. Any bubble attaining this point will change its direction of travel and move upward in the water tank. Due to the instability of the plume, a series of 2,727 images were necessary to obtain accurate statistically meaningful position in the average image. Using the image analysis procedure described in the previous section, the penetration depth H_p as a function of impact velocity V_j and for three jet outlet velocities as a parameter is plotted in Figure 5.

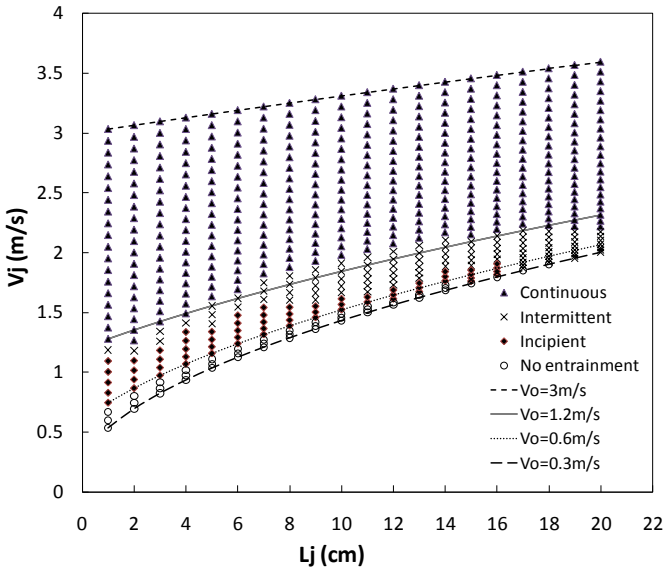

Figure 4: Flowmap regimes – Entrainment regimes depending on jet length L_j and impact velocity V_j.

The overall variation of the penetration depth is similar for two impact velocity conditions (2 and 2.5 m/s). The Penetration depth decreases exponentially when V_j is increased, until it reaches a constant penetration depth of about 14.5 cm and 13 cm for V_0 of 2.5 and 2 m/s respectively. The penetration depth is longer for a higher impact velocity. For V_0=1.5 m/s the trend is fundamentally different.

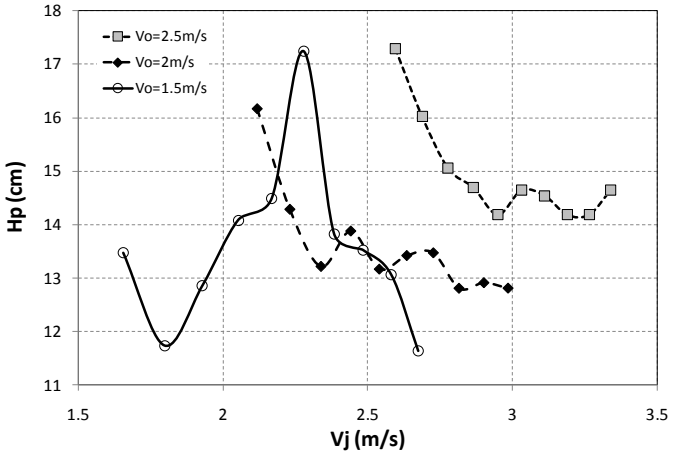

Note: The penetration depth was obtained for L_j ranging from 2.5 cm to 25 cm.

Figure 5: Penetration Depth H_p for continuous entrainment as a function of jet velocity V_j.

2D Velocity Distribution

To characterize the no-entrainment flow, the velocity vector field below the pool free surface in the vertical plane was measured by post processing of the particle images using PIV (Figure 6). The no entrainment regime was chosen

because it is amenable to easy optical access by the transmission and reception optics of the PIV.

Far from the interface and in the center region of the tank, the fluid particles are entrained to the bottom of the tank with an average velocity of 0.047 m/s. The jet core velocity accelerates just after impingement on the liquid free surface and proceeds downwards to impinge on the bottom surface of the tank. At the bottom, the jet deflects towards the sidewalls thus generating two symmetrical vortices circulating in opposite direction.

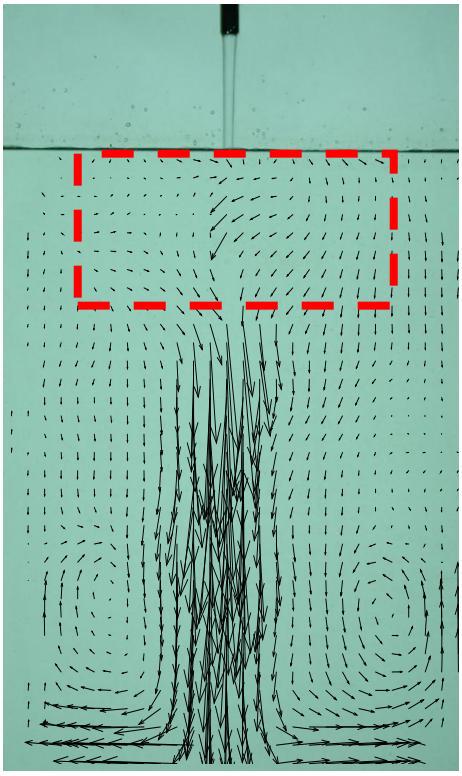

Figure 6: Averaged velocity distribution inside the tank for no-entrainment flow.

Below the horizontal interface where the jet enters the water, the averaged velocity distribution is not structured and the flow pattern displays some skewness and entrainment from the quiescent surrounding water. The averaged velocity distribution is not uniform in this region due to the instantaneous characteristics of the jet inside the liquid. In order to understand this region a zoomed and instantaneous velocity distribution is measured using PIV (Figure 7).The instantaneous velocity distribution clearly shows changes in the jet path and cross stream area when it enters the liquid at interface suggesting buckling of the liquid column. This might be due to the roll up of the shear layer of the jet as it enters into the fluid pool due to Kelvin-Helmholtz instabilities. This could explain the skweness in the jet velocity vectors and the regions of acceleration and deceleration along the mean jet centerline. Investigation is in progress to understand and quantify better this behavior.

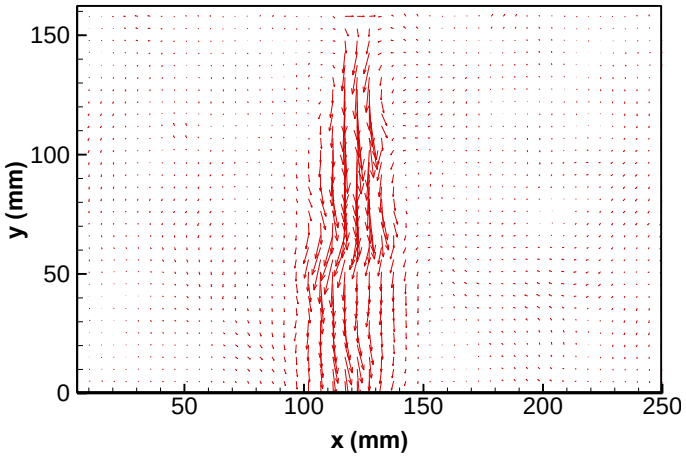

(a) t=0s

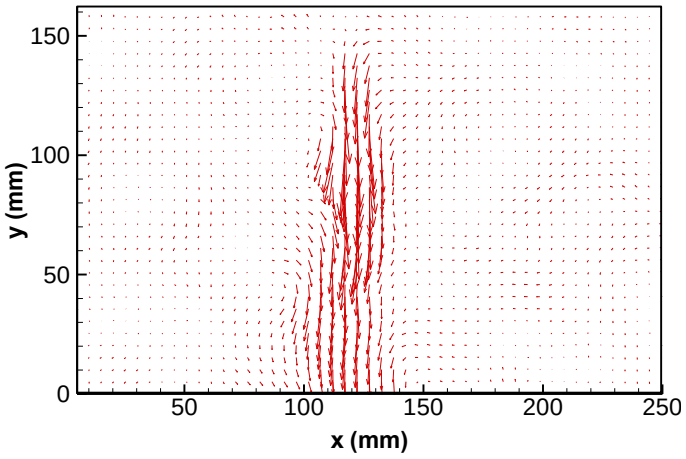

(b) t=0.2s

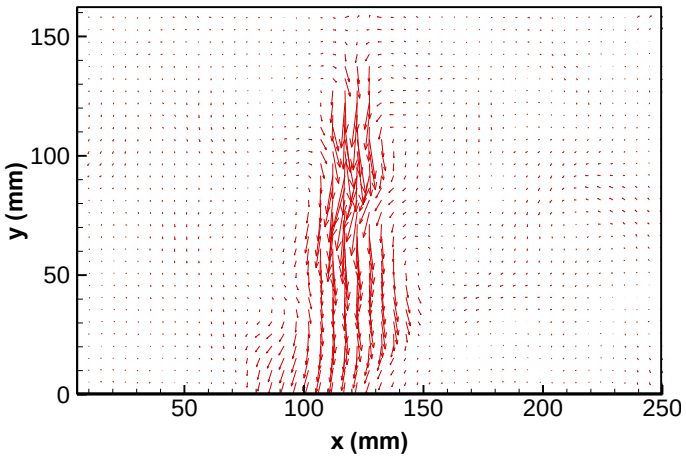

(c) t=0.4s

Figure 7: Velocity distribution of oscillatory region of the impinging jet for no-entrainment flow.

CONCLUSIONS

An experimental study was conducted to characterize a liquid impinging jet on a pool and the resulting entrainment process using non-invasive flow visualization techniques. The following conclusions may be made:

- The experimental results obtained are in full agreement with previously published work, although the range considered is wider but with some overlap.
- The penetration depth of plume for the continuous entrainment depends strongly on the jet exit velocity and decreases when the jet impact velocity increases.
- The 2D velocity distribution of the impinging jet below the interface for the no-entrainment regime was obtained. The instantaneous flow dynamic behavior of the impinging jet near and below the interface is characterized using PIV. These results would be very useful for testing CFD models.
- Future studies will be focused on the influence of control parameters such as jet length, the jet velocity and the nature of the fluid on the jet structure, its penetration and entrainment and velocities of bubbles below the interface.

REFERENCES

[1] Bin, A.K., 1993. "Gas entrainment by plunging jets" *Chemical Engineering Science*, **48**(21), pp. 3585-3630.

[2] Schmidtke, M., Danciu, D., Lucas, D., 2009, "Air entrainment by impinging jets. Experimental identification of the key phenomena and approaches for their simulation in CFD". In *Proceedings of the 17th International Conference on Nuclear Engineering (ICONE17)*, Brussels, Belgium.

[3] Bonetto, F., Lahey, R.T., 1993." An experimental study on air carryunder due to a plunging liquid jet" *International Journal of Multiphase Flow*, **19**(2), pp. 281–294.

[4] Chirichella, D., Gomez Ledesma, R., Kiger, K.T., Duncana, J.H., 2002. "Incipient air entrainment in a translating axisymmetric plunging laminar jet". *Physics of Fluids*, **14**(2), pp. 781-790.

[5] Richards, J.R., Beris, A.N., Lenhof, A.M., 1993. "Steady laminar flow of liquid-liquid jets at high Reynolds numbers". *Phys. Fluids*, **5**(1993), pp. 1703–17.

[6] Richards, J.R., Lenhof, A.M., Beris, A.N., 1994. "Dynamic breakup of liquid-liquid jets" *Phys. Fluids*, **6**(1994), pp. 2640–55.

[7] Sene, K.J., 1984. *Aspects of bubbly two-phase flow*, Ph.D. Thesis, Trinity College, Cambridge, UK, December.

[8] Schmidtke, M., Lucas, D., 2009. "CFD approaches for modeling bubble entrainment by impinging jets". *Sci. Techmn. Nucl. Inst.*, article ID148436.

[9] Raffle, M., Willert, C., Werely, S., Kompenhans, J., 2007, *Particle Image Velocimetry — A Practical Guide*, Springer, Berlin, Germany.